Efficient injection of an intense positron beam into a dipole magnetic field

2015 New J. Phys. 17 103038

(http://iopscience.iop.org/1367-2630/17/10/103038)

New Journal of Physics
The open access journal at the forefront of physics

Deutsche Physikalische Gesellschaft DPG
IOP Institute of Physics

Published in partnership with: Deutsche Physikalische Gesellschaft and the Institute of Physics

OPEN ACCESS

RECEIVED
17 August 2015

ACCEPTED FOR PUBLICATION
21 September 2015

PUBLISHED
19 October 2015

PAPER

Efficient injection of an intense positron beam into a dipole magnetic field

H Saitoh[1,2], J Stanja[1], E V Stenson[1], U Hergenhahn[1], H Niemann[1,3], T Sunn Pedersen[1,3], M R Stoneking[1,4], C Piochacz[5] and C Hugenschmidt[5]

[1] Max Planck Institute for Plasma Physics, Greifswald and Garching, Germany
[2] The University of Tokyo, Kashiwa, Japan
[3] Ernst-Moritz-Arndt-Universität Greifswald, Greifswald, Germany
[4] Lawrence University, Appleton, USA
[5] Technische Universität München, Garching, Germany

E-mail: haruhiko.saitoh@ipp.mpg.de

Keywords: antimatter plasma, electron–positron plasma, pair plasma, positron beam, dipole magnetic field

Abstract

We have demonstrated efficient injection and trapping of a cold positron beam in a dipole magnetic field configuration. The intense 5 eV positron beam was provided by the NEutron induced POsitron source MUniCh facility at the Heinz Maier-Leibnitz Zentrum, and transported into the confinement region of the dipole field trap generated by a supported, permanent magnet with 0.6 T strength at the pole faces. We achieved transport into the region of field lines that do not intersect the outer wall using the $\mathbf{E} \times \mathbf{B}$ drift of the positron beam between a pair of tailored plates that created the electric field. We present evidence that up to 38% of the beam particles are able to reach the intended confinement region and make at least a 180° rotation around the magnet where they annihilate on an insertable target. When the target is removed and the $\mathbf{E} \times \mathbf{B}$ plate voltages are switched off, confinement of a small population persists for on the order of 1 ms. These results lend optimism to our larger aims to apply a magnetic dipole field configuration for trapping of both positrons and electrons in order to test predictions of the unique properties of a pair plasma.

1. Introduction

The unusual confinement properties of a dipole magnetic field for charged particles were first recognized in the context of planetary magnetospheres. Among them is a tendency of the charged particle density profile to become steeper by inward diffusion [1–3]. Contrary to most other devices, a dipole magnetic field is suitable for storing both neutral and non-neutral plasma by external fields alone [4, 5]. Besides being of interest in its own right, this field configuration is therefore an excellent candidate for the storage of a neutral pair plasma consisting of only electrons and positrons. If this type of plasma could be created and confined in a laboratory, predictions are that it would have quite unusual properties not hitherto observed in conventional plasma [6].

In studies of the magnetic confinement of conventional plasma, the plasma is typically produced by ionization of neutral gas. For an electron–positron plasma, the analogous process would require dissociation of positronium (Ps), which indeed has been suggested [7]. The production of significant quantities of Ps is an active area of research [8], and may need several years of dedicated work before reaching maturity.

A more basic prerequisite is the availability of sufficient numbers of positrons. Currently, the most intense positron sources use a neutron capture reaction and subsequent pair production from energetic γ ray photons at a nuclear reactor to produce a directed, mono-energetic positron beam. One example is the NEutron induced POsitron source MUniCh (NEPOMUC) facility at the Heinz Maier-Leibnitz Zentrum (MLZ) in Munich, Germany [9]. In order to generate pair plasmas in a closed field line trap, we have to transport on the order of 10^{10} positrons (and electrons) across field lines. Prior to the construction of a superconducting accumulator and trap system for the creation of pair plasmas [7], we are conducting proof-of-principle studies on the injection

schemes using a prototype dipole field trap generated by a permanent magnet. Here, we describe experiments in which we inject the positron beam from NEPOMUC into the confinement region of a magnetic dipole field in the prototype device. This result is a key step required for creating an electron–positron plasma in this type of field.

Injection of charged particles into a magnetic dipole field has been studied in a number of experiments in a geophysical context, the earliest of them dating back to the turn of the last century [10]. Most often, a spherical magnetic dipole, sometimes called 'terrella' (little Earth), was used. Early work in this direction has been summarized in [11] and more recent results are, for example, in [12]. Here, we consider a slightly different idea, namely to manipulate particle trajectories using a tailored, static electric field to inject particles into the confinement region via the $\mathbf{E} \times \mathbf{B}$ drift. This idea has been considered for adding positrons to an electron plasma trapped in a stellarator, and injection has been made plausible by numerical simulations [13]. We are not aware of any prior experimental demonstration of this scheme.

The trajectories of particles confined in dipole magnetic fields have also been studied, both in the context of terrella experiments [14] and in basic research on nuclear fusion. Of greatest relevance here are studies on pure electron plasmas in the field of a levitated, superconducting current loop (RT-1) [15], which achieved confinement for up to 300 s [5, 16]. Recently, it has been also reported that a significant population of antiprotons is confined in Earth's magnetosphere [17, 18].

2. Experimental setup

Our experiments, which are part of A Positron-Electron eXperiment (APEX) project, were conducted at the open beam port of NEPOMUC [9]. At NEPOMUC, the thermalized neutrons from the research reactor ForschungsReaktor München II (FRM II) are used to create high-energy γ radiation via the nuclear reaction ^{113}Cd(n, γ) ^{114}Cd. Positrons are generated by pair production in a Pt structure located in the tip of a beam tube. Subsequent moderation in Pt leads to the emission of monoenergetic positrons at the surface. Electric and magnetic fields are used to form a bright and monoenergetic positron beam, in which the bias of the Pt foil determines the kinetic energy of the positron beam. After a recent upgrade, NEPOMUC delivers more than 10^9 moderated positrons per second [19]. Most of the experiments conducted at the NEPOMUC benefit from brightness enhancement, which is generated outside the reactor shielding by focusing the primary positron beam onto a tungsten single crystal and subsequent (re-)moderation inside the crystal. By biasing the crystal and adjusting the extraction fields, the energy of the remoderated positron beam can be set in a wide range between 5 and 300 eV. The remoderated beam has an enhanced phase space density, and due to the high efficiency of the device still contains 5%–10% of the original particle flux.

A sketch of the experimental setup is shown in figure 1. In operation, two turbomolecular pumps (not shown) evacuate the apparatus to a base pressure of 7×10^{-6} Pa. The positron beam in the NEPOMUC beamline is magnetically guided with a field of typically 5 mT. A set of Helmholtz coils provides matching of the guiding field up to the entrance of the experimental chamber (see figure 1(a)). Upstream of the entry point, additional correction coils (8×10 cm rectangular shape and 15 turns) allow two-dimensional steering of the beam propagation direction. Centrally located in the main vacuum chamber, a permanent neodymium magnet with a field of 0.6 T at its surface is positioned in a copper case. Above the magnet, a pair of non-magnetic stainless-steel $\mathbf{E} \times \mathbf{B}$ plates produce a static electric field orthogonal to the magnetic guiding field. Each of the plates is biased to $V = \pm V_{\mathbf{E}\times\mathbf{B}}$ with respect to the chamber wall. Directions of magnetic field lines and of the $\mathbf{E} \times \mathbf{B}$ drift are shown in the figure. The magnet case and an electrically connected supporting rod are insulated from the chamber in order to apply a bias potential V_{mag}. For control of injection and confinement properties, a cylindrical outer electrode with a diameter of 18 cm and height of 30 cm is installed and is biased to V_{oe}. At the equator of the trap chamber on the opposite side of the magnet from the $\mathbf{E} \times \mathbf{B}$ plates, a movable target probe is placed for the direct detection of positrons in the confinement region. The target tip is a 1 cm $\times$ 1 cm non-magnetic stainless-steel plate and connected to a supporting rod. The tip and supporting rod are electrically insulated from the chamber and can be used as a positron current collector. At the connection to the open beam port (the topmost part shown in the sketch), an insulated copper cylinder is located in the beam tube, which permits rapid blocking of the positron beam by applying an electric potential using a solid-state switch.

A top view of the experiment is shown in figure 1(b). In our experiment, positrons were detected by observing annihilation γ ray photons from two different positions: first from the movable target probe (and part of the outer electrode) and second from the top of the magnet case. Two scintillation detectors (BGO crystals of 22 mm diameter and 25 mm length from Korth Kristalle with Hamamatsu H10425 photomultipliers) were used, whose viewing angles were limited by arrangements of lead bricks. The detector signals were processed with Ortec 855 amplifiers and 551 timing SCAs, and the numbers of 511 keV γ ray were recorded with Canberra

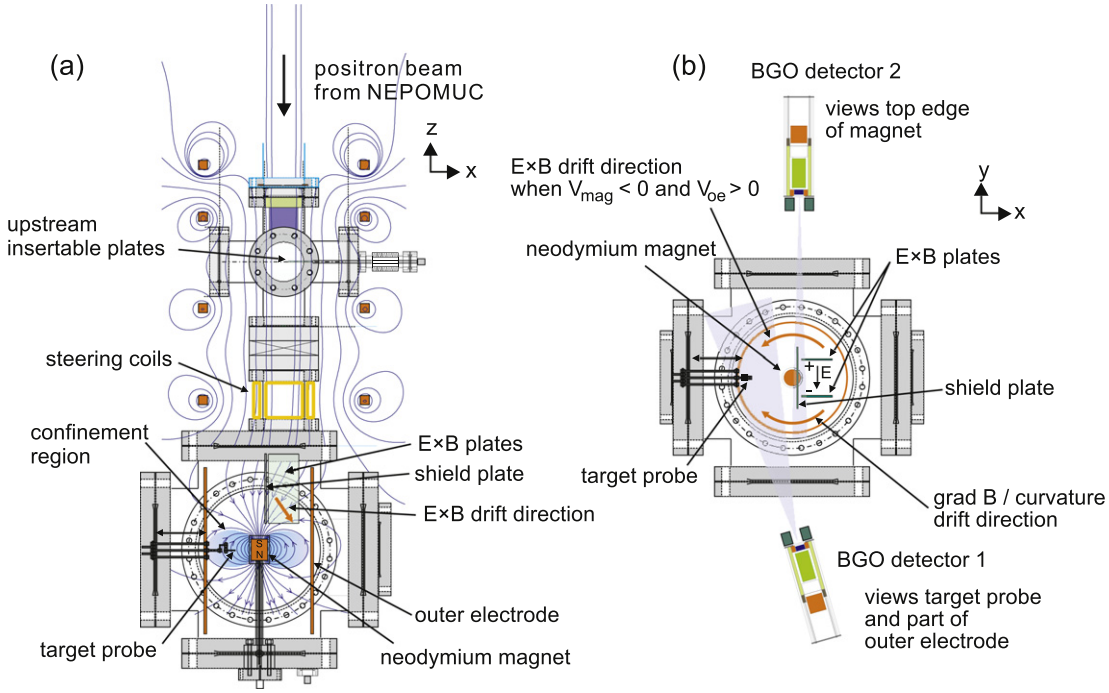

Figure 1. Sketch of the experimental set-up. (a) A side view of the vacuum chamber and the interface to the NEPOMUC positron beam at the open beamport. Blue lines show magnetic field lines. (b) Top view of the main chamber, showing the viewing angles of the two scintillation detectors used to monitor positron injection.

2071 A digital counters. In the following, these will be referred to as BGO 1 (viewing the target) and 2 (viewing the magnet case).

3. Trajectory calculations

The field strength of the permanent magnet greatly exceeds the guiding field in the beamline. Without the application of appropriately adjusted external fields, most positrons are reflected back up the beamline, due to magnetic mirroring or are simply lost by hitting the magnet case. Because of that, it is not clear *a priori*, whether a significant fraction of the positrons can enter the confinement region at all. In order to develop ways around this problem (and because of less than satisfactory results from a first set of experiments), we have done detailed trajectory simulations of positrons in the applied electric and magnetic fields. By doing so, we have found a configuration of electric field elements which appears promising. Simulations have been done using the SIMION programme [20], with a spatial grid density of 1 mm in a non-axisymmetric magnetic field generated by combination of field coils and the permanent magnet as well as realistic electrostatic boundary conditions. Calculations neglected interactions of positrons with each other, and with charged or neutral background particles. This is justified because of the low density of the remoderated positron beam.

Typical results of the calculations are shown in figure 2. A 5 eV positron with a velocity ratio of $v_x : v_y : v_z = 0.3 : 0 : -1$ was injected into the dipole trap from the beamline. When the $\mathbf{E} \times \mathbf{B}$ plates are not biased, the positron is guided towards the top of the magnet, where most of the field lines in the beamline converge due to the strong field gradient. When the particle is not in the loss cone, it is reflected due to the mirror effects (orbit 1 in the figure). By biasing the $\mathbf{E} \times \mathbf{B}$ plates so that the radial drift is directed towards the confinement region (see figure 1 for the bias polarity and field direction), the particle drifts inward and onto field lines in the confinement region (orbit 2). When an appropriate $V_{\mathbf{E}\times\mathbf{B}}$ is not applied, positrons are not injected into the confinement region, but are lost mainly by hitting the outer electrode (orbit 3). Our results show that particles may enter into the magnetic dipole field and be mirror trapped without hitting the magnet case, and will precess toroidally around the magnet while bouncing up and down along the magnetic field lines. The typical toroidal rotation frequency due to the precession motion is a few tens of kHz (see below).

After being successfully injected from the beamline, a positron is confined in the trap until it is lost on the surfaces of magnet case, outer electrode, or other electrodes. As shown in figure 3, the flight time of a positron depends on the pitch angle of a particle as well as on $V_{\mathbf{E}\times\mathbf{B}}$. When $v_x : v_y : v_z = 0 : 0 : -1$ and $0.1 : 0 : -1$, as shown with solid and dot lines in the figure, the particle is in the loss cone and is lost on the magnet case just after it drifts close to the magnet. On the other hand, effective drift injection into the confinement region is realized by

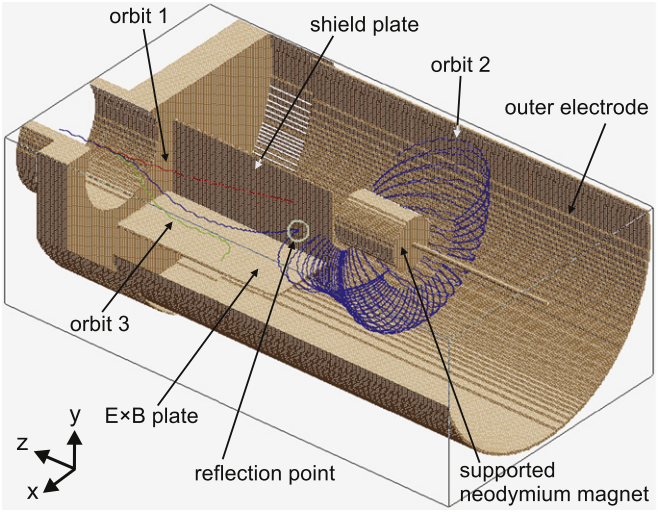

Figure 2. Typical trajectories of a 5 eV positron with an initial velocity ratio of $v_x : v_y : v_z = 0.3 : 0 : -1.0$. Without the application of $\mathbf{E} \times \mathbf{B}$ plate bias ($V_{\mathbf{E}\times\mathbf{B}} = 0$ V, orbit 1), the positron is lost by reflecting back up the beamline by magnetic mirror. When the $\mathbf{E} \times \mathbf{B}$ plates are biased to $V_{\mathbf{E}\times\mathbf{B}} = 95$ V (orbit 2), the positron is transported across field lines and injected into the confinement region. When $V_{\mathbf{E}\times\mathbf{B}} = 150$ V (orbit 3), the positron is not injected to the dipole field and is lost on the outer electrode. The shield electrode and the magnet case were set to 0 V against the chamber. One of the $\mathbf{E} \times \mathbf{B}$ electrodes is not shown.

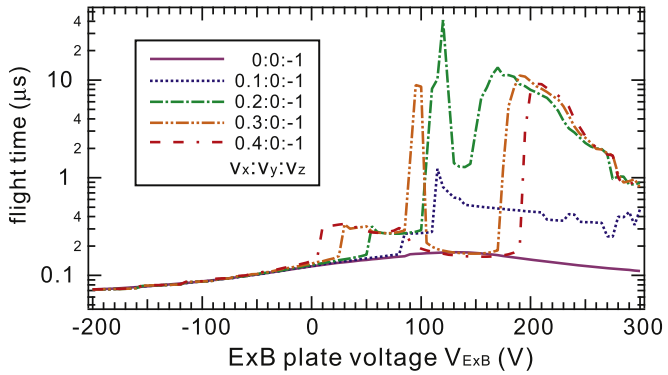

Figure 3. Simulated flight time of positrons in the dipole trap as a function of $V_{\mathbf{E}\times\mathbf{B}}$. A positron with an energy of 5 eV was injected with different velocity ratios in the parallel (z) and perpendicular (x) directions. By positively (see figure 1 for the polarity) biasing the $V_{\mathbf{E}\times\mathbf{B}}$ plates, some positrons are transported into toroidal precession orbits, which exhibit relatively long flight times.

the application of a wide range of positive $V_{\mathbf{E}\times\mathbf{B}}$ values when $v_x \geqslant 0.2$. Because of the strongly inhomogeneous field strength and rather complicated chamber and electrode geometries, the flight time shows non-linear behaviour with variation of $V_{\mathbf{E}\times\mathbf{B}}$. It is expected that several tens of percent of injected particles are guided into the confinement region, for a positron beam with finite perpendicular temperature [21].

While doing these simulations, we have noted that shielding of the stray electric field produced by the pair of $\mathbf{E} \times \mathbf{B}$ plates is important. Without reducing the stray fields, the particle orbits tend to expand during the precession motion, resulting in early annihilation of particles on the outer electrode. In order to prevent these effects, the grounded shielding electrode, seen near the magnet in figures 1 and 2, has been added in the experiment.

In order to quantify the injection efficiency and loss channels numerically, 1000 positrons were injected from the beamline into the trap (figure 4). In this calculation, we set $V_{\mathbf{E}\times\mathbf{B}} = 100$ V and $V_{\mathrm{mag}} = V_{\mathrm{oe}} = 0$ V. The positrons were given a randomized set of perpendicular energies as explained in the figure caption. When the target probe is retracted, the main loss channels are the outer electrode and the magnet case, as expected from the particle properties described above. By placing the target probe in the confinement region, some particles are lost at the target after making a 180° toroidal rotation in the dipole field, instead of hitting the magnet case or outer electrode. Because the toroidal precession velocity was slow enough compared with the bounce motion, all positrons are lost on the target when they cross the same r–z cross section as that of the target probe. Therefore it is expected that we can effectively detect positrons after the initial half toroidal rotation at the target.

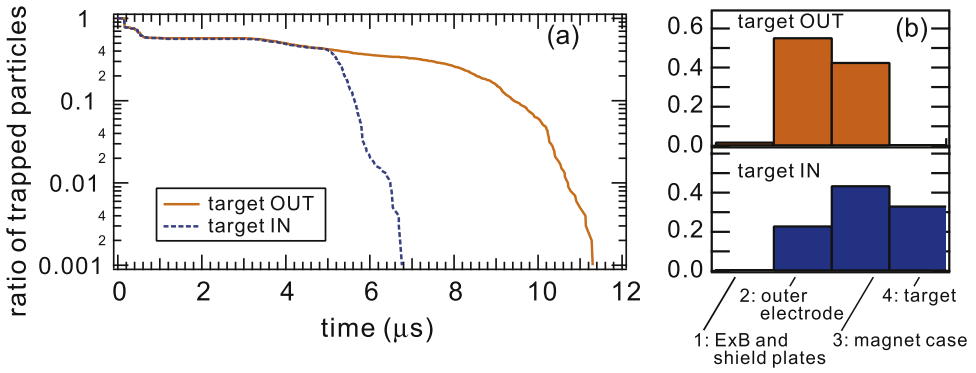

Figure 4. (a) Fraction of confined positrons versus time with the target probe inserted and retracted (simulated results). At $t = 0$ s, 1000 positrons with a kinetic energy of 5 eV were injected into the trap. The velocity ratio was $v_x : v_y : v_z = v_a : v_b : -1$, where v_a and v_b were distributed randomly between −0.2 and 0.2. (b) Ratio of positrons lost at (1) $\mathbf{E} \times \mathbf{B}$ and shield plates, (2) outer electrode, (3) magnet case, and (4) target plate, for the cases when the target is retracted (top) and inserted (bottom).

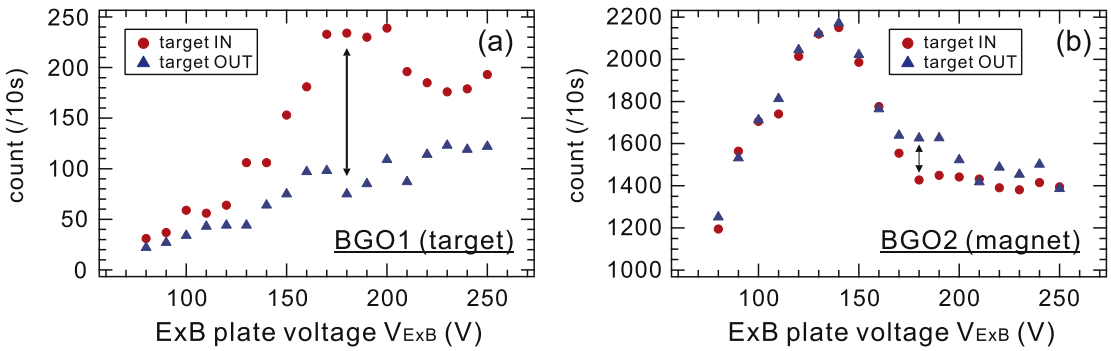

Figure 5. Counts on the scintillation detectors monitoring the target probe (a) and the top of the permanent magnet (b) with the $\mathbf{E} \times \mathbf{B}$ plates set to $\pm V_{\mathbf{E}\times\mathbf{B}}$. Circles denote measurements with the target probe inserted, triangles with the target probe retracted. A beam energy of 5 eV was used. Accumulation time was 10 s. The magnet case was biased to $V_{mag} = -15$ V and the outer electrode to $V_{oe} = 5.5$ V.

4. Experimental results

4.1. Particle injection into the dipole field

Guided by these simulations, we have conducted experiments to test this injection scheme. We have found that besides optimizing $V_{\mathbf{E}\times\mathbf{B}}$, the steering coil current and the bias voltages on the magnet case (V_{mag}) and the outer electrode (V_{oe}) had a strong influence on the results. Effective injection was realized by applying $V_{oe} = 5.5$ V, which was just above the positron beam energy of 5 eV. For a given setting of the steering coils, we show results for positron injection as a function of $V_{\mathbf{E}\times\mathbf{B}}$ in figure 5 and as a function of V_{mag} in figure 6. In both figures, the left panel shows annihilation counts from the detector viewing the retractable positron target. As positrons have to precess around the magnet by 180° before annihilating on this plate, we interpret a surplus of annihilation counts from this target in its 'in' position as a signature of positron injection into the confinement region. Since the detector does not exclusively view the target area, it is useful to compare annihilation counts with the target in its 'in' and 'out' positions. Figures 5 and 6 indeed show a significant increase of the annihilation counts when the target is inserted, which is strongest for settings of around $V_{\mathbf{E}\times\mathbf{B}} = 180$ V and a magnet bias of $V_{mag} = -15$ V. These settings are marked with black arrows in figures 5 and 6. Observing good injection conditions at these values of the parameters is in reasonable agreement with our simulations, as explained in the next subsection.

A cross-check of our interpretation is possible by comparing annihilation on the target probe to annihilation on the magnet case (panel (b) in both figures). For the conditions we found optimal, it is seen that the increase of particles annihilating on the target is accompanied by a decrease of particles observed on the magnet, always measured relative to the count rate with retracted target. This can only be the case if those positrons, that are injected into the magnetic field when the target is retracted, make even longer trajectories—trajectories that

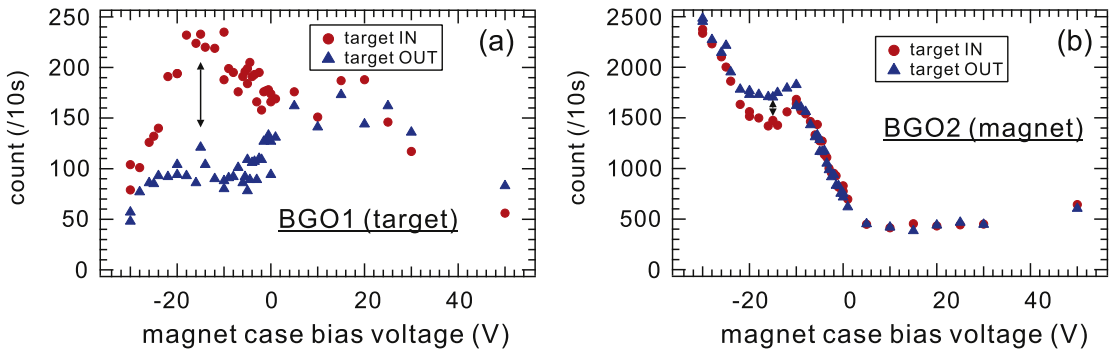

Figure 6. Same as figure 5, for variable bias of the magnet case. $V_{\mathbf{E}\times\mathbf{B}} = 180$ V. The outer electrode was set to $V_{oe} = 5.5$ V.

cross the azimuthal region of the target probe and reenter the solid angle observed by detector 2. This is consistent with numerical results shown in figure 4.

4.2. Toroidal drift motion

While the dependence of our results on the value of $V_{\mathbf{E}\times\mathbf{B}}$ is expected and quite natural, the dependence on the bias of the magnet case requires some explanation. A charged particle in a magnetic dipole field undergoes gyromotion around the field lines, and bounce motion between regions of high magnetic fields near the poles (see figure 2). Additionally, the guiding centres of the gyrating motion of the particles experience a toroidal drift motion around the magnet. Three mechanisms cause these drift motions [22]. Two of them are the curvature drift and grad-B drift, which are the first and second terms of

$$\mathbf{v}_d = \frac{2W_{\parallel} + W_{\perp}}{qB} \frac{\mathbf{R}_c \times \mathbf{B}}{R_c^2 B}, \tag{1}$$

in the limit of negligible volumetric currents. Here q is the charge, $\mathbf{B}$ the magnetic field, $B = |\mathbf{B}|$, $W_{\parallel}$ and $W_{\perp}$ the kinetic energies of motion parallel and perpendicular to $\mathbf{B}$, $\mathbf{R}_c$ the radius of curvature vector for the field line, pointing outward from its centre of curvature, and $R_c = |\mathbf{R}_c|$. We aim for an order of magnitude estimate of the drift frequency f_d of positrons, precessing around the magnet at distance r from the axis of the magnetic dipole. We approximate that $r \approx 2R_c$ in the dipole field. Inserting $q = e$ into (1), we have

$$f_d \approx \frac{2W_{\parallel} + W_{\perp}}{\pi r^2 eB}. \tag{2}$$

Note that the ratio of $W_{\parallel}$ to $W_{\perp}$ is different for each particle, therefore although all particles experience both types of drift, the respective contributions to the drift are different. In our case, $W_{\parallel}$ is greater than $W_{\perp}$ and the curvature drift dominates. For the strength of our permanent magnet, we obtain an approximate precession frequency of $f_d = 60$ kHz for 5 eV positrons at a radial position of 5 cm (where $B \sim 20$ mT).

An additional toroidal drift occurs when an electric field is produced by biasing the magnet with respect to the outer electrode, $\mathbf{E} \times \mathbf{B}/B^2$. For a potential difference ΔV between the magnet and the electrode, this drift takes the approximate form

$$f_{\mathbf{E}\times\mathbf{B}} = \frac{F\Delta V}{2\pi r^2 B}, \tag{3}$$

where F is a geometrical factor of order $\ln(b/a)$. Here a is the radius of the magnet and b is the radius of the outer electrode. The sense of rotation of this toroidal drift depends on the sign of the electric field. In other words, by biasing the magnet and outer electrode appropriately, we can practically cancel or enhance the toroidal drift due to the magnetic effects outlined above. For the example above, a potential difference of approximately $\Delta V = -10$ V is sufficient to cancel the magnetic drifts.

We have numerically calculated the positron orbits in approximately the geometry of our experiment, in order to assess the effects of magnet case and outer electrode bias. In figure 7, the fraction of trapped particles is plotted for the set of V_{mag} and V_{oe} after 5, 10, 20, and 50 μs from injection. In all cases, the ratio $V_{mag} : V_{oe} = -15 : 5.5$, so that the $\mathbf{E} \times \mathbf{B}$ drift velocity varied but the electrostatic potential in the confinement region did not greatly change in each of the calculations. For each data set, 200 positrons with a kinetic energy of 5 eV were injected at $t = 0$ s with random perpendicular energies satisfying ν_a, $\nu_b \leqslant 0.4$, where $\nu_x : \nu_y : \nu_z = \nu_a : \nu_b : -1$. The dependence of the trap time on V_{mag} is explained as follows: The radial electric field, generated by a potential difference between the magnet case and the outer electrode, is distorted by the effects of the $\mathbf{E} \times \mathbf{B}$ and shield plates. Some particles are lost by vertically drifting outward due to the error

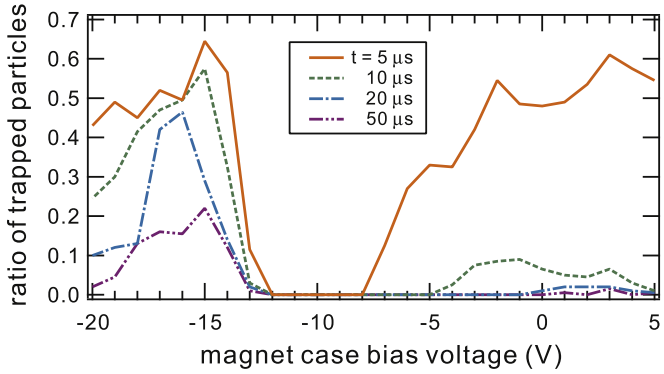

Figure 7. Fraction of simulated trapped positrons (integrated from probe position to outer electrode) after 5, 10, 20, and 50 μs following injection as a function of V_{mag} and outer electrode V_{oe} . The ratio of V_{mag} and V_{oe} was kept to be −15 :5.5. 200 particles were randomly injected for each of the calculation conditions.

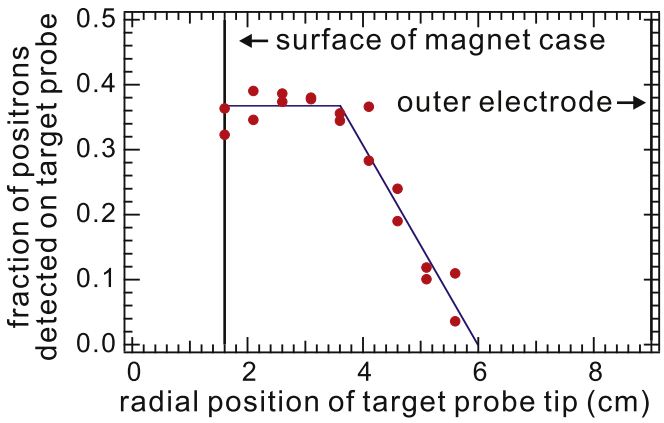

Figure 8. Positron current measured on the target probe as a function of radial position. Current is expressed as a fraction of the current measured on the insertable plate, upstream of the steering coils (see figure 1(a)). Bias voltages were set to the optimized values, as given in the text.

electric field in the azimuthal direction. When $-12\ \text{V} < V_{mag} < -5\ \text{V}$ in figure 7, such a loss mechanism as well as expansion toward the outer electrode is dominant, resulting in short confinement. By further biasing the magnet case negatively, the cancellation of magnetic drift precession motion results in relatively long trap times. When the magnet is biased below $V_{mag} < -13\ \text{V}$, more particles have relatively long flight times compared to the case with $V_{mag} = 0\ \text{V}$.

Given the above, we interpret the enhancement of annihilation counts at the target for negative magnet bias as being caused by a cancellation of the magnetic drift motion by the $\mathbf{E} \times \mathbf{B}$ drift, which seems to reduce the outward drift of the positrons and subsequent loss on the outer electrode. It is also possible that for some positrons the field is sufficiently strong to reverse the direction of toroidal precession, such that they reach the annihilation plate from the other side. Why this would lead to an increase in signal remains to be clarified by further experiments focusing on the effects of electrode bias and steering coil currents.

4.3. Positron current and injection efficiency

The positron flux measured on the 'upstream insertable plate' (figure 1(a)) using a current integrating amplifier amounted to $(2.3 \pm 0.2) \times 10^7/\,\text{s}$ for a 5 eV beam [21]. The actual beam current may be up to a factor of approximately two times higher due to reflection of positrons by the plate. The positron current measured on the retractable target probe as a function of the radial position is shown in figure 8. The target probe collects positrons on orbits that intersect the probe and its shaft, extending to the outer wall. Results show that positrons are distributed between a radial position of 3.5 and 6.9 cm from the axis of the magnet in the confinement region. Saturation of the measured current at smaller distances shows that the positrons do not reach this higher field region. These measurements show that about 38 % of the positrons are able to reach the closed field region and make at least one half turn around the magnet.

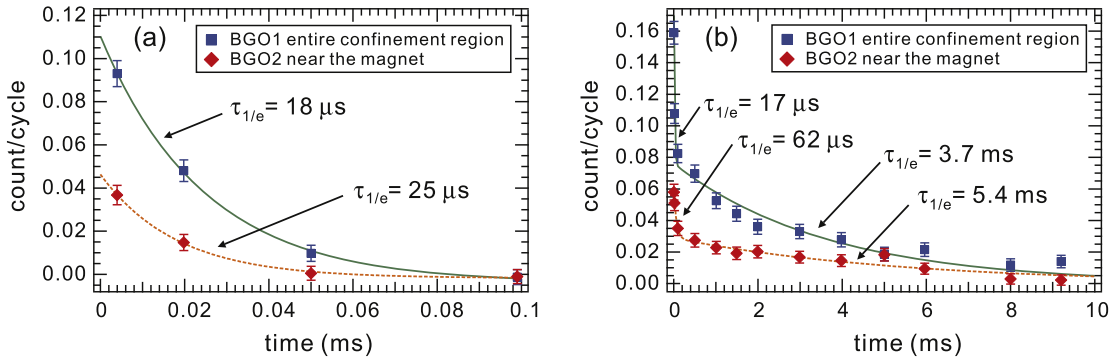

Figure 9. Counts measured with scintillation detector 1 (viewing the whole dipole region, squares) and detector 2 (viewing near the magnet, diamonds) (a) when dc voltage of $V_{\mathbf{E}\times\mathbf{B}}$= 180 V was applied to the $\mathbf{E} \times \mathbf{B}$ plates and (b) when $V_{\mathbf{E}\times\mathbf{B}}$= 180 V was applied only during injection. Decay time constants were obtained by (a) exponential and (b) double exponential fitting of the data. The magnet case and outer electrode were biased to $V_{\mathrm{mag}} = -14$ V and $V_{\mathrm{oe}} = 6$ V.

4.4. Lifetime

We determined the lifetime of the positron cloud in the dipole trap by turning off the positron beam with a fast switch on an upstream bias electrode. We then used a scintillation detector observing the whole target chamber, to measure annihilation counts as a function of delay time Δt after the beam was blocked. After blocking the beam at $t = 0$ s (the rise time of electrode voltage was less than 200 ns), we measured the annihilation counts from $t = \Delta t$ to $\Delta t + 10$ ms. The data were accumulated over 4000 inject-block-count cycles for each value of Δt. The detected counts per cycle as a function of Δt are plotted in figure 9. Background levels were subtracted using data measured in a similar manner but with the positron beam electrostatically blocked. In these experiments, scintillation detectors viewed the entire confinement region (BGO 1) or more localized area near the magnet (BGO 2). When we applied dc $V_{\mathbf{E}\times\mathbf{B}}$ for the entire cycle, the observed lifetimes τ were 18 μs (BGO 1) and 25 μs (BGO 2), as shown in figure 9(a), which are comparable to the toroidal precession time due to the cross-field drifts, indicating that particles survive, on average, about one toroidal precession orbit.

Asymmetric fields used to inject positrons from the beamline may be responsible for ejection of positrons after one toroidal precession. We tested this hypothesis by switching off the positron beam upstream, simultaneous to switching off the bias on the $\mathbf{E} \times \mathbf{B}$ plates, and subsequently measure the confinement of the injected positrons. As shown in figure 9(b), we observed a decay characterized by two different time constants, one of which was much longer than in the cases when dc $V_{\mathbf{E}\times\mathbf{B}}$ voltages were applied. The longer confinement times were 3.7 ms (BGO 1) and 5.4 ms (BGO 2), implying that injected positrons survived for many toroidal rotation periods in the dipole field. The decay times observed by BGO 2 were longer than the BGO 1 data, which is consistent with the long-lived positron component being distributed in a strong magnetic field region.

Besides the positron beam injection experiments detailed above, we have also performed test experiments, in which an electron beam from a heated filament was injected into the same dipole field. In those experiments, lifetimes in the 100 ms range were observed, indicating that the permanent magnet dipole device has a much longer confinement capability for single component charged particles. It is possible that further optimization of positron injection scheme results in improved confinement properties. In order to further transport positrons into the confinement region and to realize a long-confinement and high-density state, we plan to apply spatially and temporally variable electric fields (i.e., a 'rotating wall') for injection in future experiments.

5. Summary

In summary, we succeeded in injecting positrons into a dipole magnetic field, produced by a supported permanent magnet. Using a static electric field to produce an $\mathbf{E} \times \mathbf{B}$ drift, we were able to transport a cold, directed positron beam from outside into the region of field lines that do not intersect the outer wall. Optimal injection conditions were obtained when the magnet was biased relative to the outer wall with a polarity such that the resulting toroidal $\mathbf{E} \times \mathbf{B}$ drift was of comparable magnitude and in the opposite direction of the curvature drift. An injection efficiency of approximately 38% was achieved, and particle lifetime in the trap was about 5 ms. For future experiments on the confinement of positrons and electrons over long times, we will construct a superconducting, levitated current loop. Besides producing a stronger confinement field, such a device eliminates the effects of field lines that intersect the poles of a permanent magnet.

Acknowledgments

The authors acknowledge contributions of Norbert Paschkowski and Sebastian Vohburger to setting up the experiment. EVS acknowledges a grant by the Helmholtz Society. This work is based upon experiments performed at the NEPOMUC positron beam facility operated by FRM II at the Heinz Maier-Leibnitz Zentrum (MLZ), Garching, Germany. This work was partially supported by JSPS Grant-in-Aid for Scientific Research 25707043.

References

[1] Hasegawa A 1987 A dipole field fusion reactor *Comments Plasma Phys. Control. Fusion* **11** 147–51
[2] Boxer A C, Bergmann R, Ellsworth J L, Garnier D T, Kesner J, Mauel M E and Woskov P 2010 Turbulent inward pinch of plasma confined by a levitated dipole magnet *Nat. Phys* **6** 207
[3] Yoshida Z, Saitoh H, Yano Y, Mikami H, Kasaoka N, Sakamoto W, Morikawa J, Furukawa M and Mahajan S M 2013 Self-organized confinement by magnetic dipole: recent results from RT-1 and theoretical modeling *Plasma Phys. Control. Fusion* **55** 014018
[4] Yoshida Z *et al* 1999 Toroidal magnetic confinement of non-neutral plasmas *AIP Conf. Proc.* **498** 397–404
[5] Yoshida Z, Saitoh H, Morikawa J, Yano Y, Watanabe S and Ogawa Y 2010 Magnetospheric vortex formation: self-organized confinement of charged particles *Phys. Rev. Lett.* **104** 235004
[6] Helander P 2014 Microstability of magnetically confined electron–positron plasmas *Phys. Rev. Lett.* **113** 135003
[7] Sunn Pedersen T, Danielson J R, Hugenschmidt C, Marx G, Sarasola X, Schauer F, Schweikhard L, Surko C M and Winkler E 2012 Plans for the creation and studies of electron–positron plasmas in a stellarator *New J. Phys.* **14** 035010
[8] Cassidy D B, Hisakado T H, Tom H W K and Mills A P 2012 Efficient production of Rydberg positronium *Phys. Rev. Lett.* **108** 043401
[9] Hugenschmidt C, Piochacz C, Reiner M and Schreckenbach K 2012 The NEPOMUC Upgrade and advanced positron beam experiments *New J. Phys.* **14** 55027
[10] Rypdal K and Brundtland T 1997 The Birkeland terrella experiments and their importance for the modern synergy of laboratory and space plasma physics *J. Physique* **07** C4–113–C4–132
[11] Schindler K 1969 Laboratory experiments related to the solar wind and the magnetosphere *Rev. Geophys.* **7** 51–75
[12] Minami S and Takeya Y 1986 Plasma injection into a simulated magnetosphere *Planet. Space Sci.* **34** 69–76
[13] Durand de Gevigney B, Sunn Pedersen T and Boozer A H 2011 Debye screening and injection of positrons across the magnetic surfaces of a pure electron plasma in a stellarator *Phys. Plasm.* **18** 013508
[14] Warren H P and Mauel M E 1995 Observation of chaotic particle transport induced by drift-resonant fluctuations in a magnetic dipole field *Phys. Rev. Lett.* **74** 1351–4
[15] Nishiura M, Yoshida Z, Saitoh H, Yano Y, Kawazura Y, Nogami T, Yamasaki M, Mushiake T and Kashyap A 2015 Improved beta (local beta >1) and density in electron cyclotron resonance heating on the RT-1 magnetosphere plasma *Nucl. Fusion* **55** 053019
[16] Saitoh H, Yoshida Z, Morikawa J, Yano Y, Hayashi H, Mizushima T, Kawai Y, Kobayashi M and Mikami H 2010 Confinement of electron plasma by levitating dipole magnet *Phys. Plasmas* **17** 112111
[17] Adriani O, Barbarino G C, Bazilevskaya G A, Bellotti R, Boezio M *et al* 2011 The discovery of geomagnetically trapped cosmic ray antiprotons *Astrophys. J.* **737** L29
[18] Schwarzschild B M 2011 A belt of magnetically trapped antiprotons girdles Earth *Phys. Today* **64N10** 16
[19] Hugenschmidt C, Ceeh H, Gigl T, Lippert F, Piochacz C, Reiner M, Schreckenbach K, Vohburger S, Weber J and Zimnik S 2014 Positron beam characteristics at NEPOMUC Upgrade *J. Phys. Conf. Ser.* **505** 012029
[20] Dahl D A 2000 SIMION for the personal computer in reflection *Int. J. Mass Spectrom.* **200** 3–25 Volume 200:The state of the field as we move into a new millenium
[21] Stanja J *et al* to be published
[22] Goldston R J and Rutherford P H 1995 *Introduction to Plasma Physics* (Bristol: IOP Publishing)